Journal of Micromechanics and Microengineering



# Highly sensitive ionic pressure sensor based on concave meniscus for electronic skin

To cite this article before publication: Qi Su *et al* 2019 *J. Micromech. Microeng.* in press https://doi.org/10.1088/1361-6439/ab5a2b

# Highly Sensitive Ionic Pressure Sensor Based on Concave Meniscus for Electronic Skin

Qi Su[1], Xian Huang[2], Kuibo Lan[1], Tao Xue[3], Wei Gao[4] and Qiang Zou[1]*

[1] School of Microelectronics, Tianjin International Joint Research Center for Internet of Things, Tianjin Key Laboratory of Imaging and Sensing Microelectronic Technology, Tianjin University, Tianjin 300072, China
E-mail: zouqiang@tju.edu.cn

[2] Department of Biomedical Engineering, Tianjin University, Tianjin 300072, China

[3] Analysis and Testing Center, Tianjin University, Tianjin 300072, China

[4] Institute of Plant Protection, Tianjin Academy of Agricultural Sciences, Tianjin 300381, China

**Keywords:** flexible electronics, pressure sensor, template molding, ionic gel

## Abstract

Flexible pressure sensing plays a critical role in the human-machine interaction therefore highly sensitive pressure sensors have promising potential in such applications. Capacitive pressure sensor has inherent attributes of simple configuration and fast response time. However, the existing applications of sensors are limited by the limited sensitivity as well as complex manufacturing. Herein, a highly sensitive ionic pressure sensor with the microstructured dielectric layer has been proposed. The polycarbonate membrane is used as the template to manufacture the microstructure of concave meniscus. By packing the top electrode, dielectric layer and bottom electrode, the ionic pressure sensor are fabricated. The sensor presents a sensitivity of 35.96 k $Pa^{-1}$ with an excellent robustness of tolerating repeated pressure for at least 200 000 cycles without fatigue. In addition, the response time of the sensor is 21 ms and

the limit of detection is 0.61 Pa. The ionic pressure sensor offers a highly sensitive sensing device for robotics and human-machine interaction. Furthermore, the concave meniscus realized by template-based method provides a novel guideline for other microstructure-enabled devices.

## 1. Introduction

Pressure sensors that convert external pressure into electric signals have been extensively investigated in research fields in artificial skin [1-3], soft robots [4-6], human-machine interaction [7,8] and health monitoring [9,10]. Among them, capacitive sensors present particular merits of simple device configuration, fast response speed, low power consumption and high sensitivity thereby being widely explored in many related applications [11,12]. In order to improve the performance of pressure sensors, various microstructures of dielectric layer have been designed and realized for lower Young' modulus, such as micropyramid [13,14], microdome [15,16], rough surface [17,18] and porosity [19,20]. Meanwhile, a number of conductive materials, such as carbon nanotubes [21] and silver nanowire [22,23] were mixed with elastomers to enhance the permittivity of dielectric layer and thus boost the performance of sensors. However, the composite is still hard to achieve promising performance for the detection of subtle stimuli.

As a preferable alternative to the dielectric layer of elastomer combining with conductive material, ionic gel was introduced as the active material of dielectric layer to achieve high performance of sensors [24,25]. Recently, a flexible capacitive skin with a new record of maximum sensitivity 41.64 $kPa^{-1}$ was obtained based on micropyramidal ionic gel by taking advantages of microstructure and the electric double layer (EDL) [14]. However, such microstructure made by photolithography typically suffers from high price and sophisticated procedures. Subsequently, a plant template was utilized to manufacture the microstructure of

microtower array of ionic gel to achieve an ionic skin with a high sensitivity of 54.3 $kPa^{-1}$ [26]. Unfortunately, most plant leaves have the disadvantage of uncontrollable curved surface, including the Calathea zebrine leaf used in this literature, which induces uncertain performance of the device. It is therefore reasonable to find a cost-effective as well as performance-controlled way to develop a dielectric layer for a pressure sensor with high performance.

Herein, we report a microstructured ionic gel film, which acts as the dielectric layer in flexible ionic pressure sensors. The microstructured ionic gel film that templated from polycarbonate template (PCTE) has concave menisci at the top of micropillar array with an average height of ~11 μm and a diameter of ~5 μm. Compared with former microstructure such as micropyramid or microcone developed by using various template molding methods [27-29], the microstructured ionic gel film templated from PCTE is cost-effective as well as performance-controlled. The flexible ionic pressure sensor exhibits a high sensitivity of 35.96 k $Pa^{-1}$ in the pressure regime of less than 0.1 kPa and a fast response time of 21 ms as well as a limit of detection (LOD) of 0.61 Pa. Significantly, the flexible ionic pressure sensor presents high mechanical robustness that can tolerate repeated pressure for at least 200 000 cycles without fatigue. The excellent performance of the sensor is mainly attributed to the ionic-electric capacitive interfaces that is typically referred as EDL, which offers remarkably higher change in capacitance than other capacitive sensors with dielectric layers of elastomer. The detailed mechanism of EDL is introduced in this work: EDL appears at the interface of meniscus edges and electrode. When a pressure is applied on the sensor and the dielectric layer is compressed, the capacitance is improved according to the area change of the EDL capacitors in parallel. That is, the contact area of microstructured dielectric layer and electrode determines the capacitance response. Also, some applications of healthcare and human-machine interaction are used to illustrate the high performance and versatility of the ionic pressure sensor. This work provides a new route to utilize microstructure of commercial membrane template to improve

the performance of ionic pressure sensors.

## 2. Experimental Section

### 2.1. Materials:

Poly(vinylidene fluoride-co-hexafluoropropylene) (P(VdF-HFP)) and 1-ethyl-3-methylimidazolium bis(trifluoromethylsulfonyl)imide ([EMIM][TFSI]) were purchased from Sigma-Aldrich. Ethanol, acetone and dichloromethane (DCM) were purchased from Sigma-Aldrich. Silver nanowires (AgNWs) (diameter: 30 nm, length: 20-30 μm, concentration: 10 mg/mL) solution was purchased from XFNANO co., Ltd. The PCTE membrane was purchased from Whatman Co., Ltd. CPI film was purchased from Shanghai Chemical Reagents Co., Ltd. The polydimethylsiloxane (PDMS) elastomer (Sylgard 184) was purchased from Dow Corning Co., Ltd.

### 2.2. Fabrication of dielectric layer:

Ionic gel was prepared by dissolving 10% P(VDF-HFP) in acetone and then by mixing with [EMIM][TFSI]. The weight ratio of P(VDF-HFP) and [EMIM][TFSI] is 5.5:4.5. Following that an uncured ionic gel layer was spin-coated on a glass substrate with 500 rpm for 3 s, a PCTE with lots of microholes was placed on top of ionic gel layer immediately. Then PCTE and the ionic gel within it was dried in vacuum oven at 80 ℃ for 24h to remove the residual solvent. After these processes, the PCTE was dissolved with DCM and the ionic dielectric layer with microstructure of concave meniscus was obtained.

### 2.3. Fabrication of Electrodes and pressure sensor:

The PDMS mixture with a base to curing agent ratio of 10:1 was prepared and spin-coated on the glass substrate of 50 × 50 $mm^2$. After curing at 80 ℃ for 4 hours, the PDMS film of ~30 μm was peeled off from the glass substrate after DCM immersion for 12 hours. Then the PDMS film was treated with ultraviolet ozone for 8 h to obtain the hydrophilic surface of PDMS film.

Following that, the AgNWs solutions was coated on the PDMS film by a Mayer rod, and then dried at room temperature for 5 hours. Following that electrodes of 10 × 20 $mm^2$ were fabricated and a Indium Tin Oxide (ITO) conductive tape was mounted on the terminals of electrodes. Subsequently, the electrode acts as top electrode was laminated onto the electrode acts as bottom electrode with the dielectrical layer of 10 × 10 $mm^2$ being in the middle of them.

2.4. Fabrication of pressure sensor array:

Colorless polyimide (CPI) film was washed by ultrasonication in deionized water and alcohol in sequence. Subsequently, AgNWs solution were rod-coated on a CPI film and then dried at room temperature for 5 hours. After that, CPI film coated with AgNWs were cut by a laser cutter (Nichia DK 7.0) and electrodes connected with conductive bridges were fabricated. Bottom electrode array consists of 100 bottom electrodes was assembled with 100 units of dielectric layer, then packed by top electrode array.

2.5. Fabrication of pressure sensor array of high spatial resolution:

Bottom and top electrode arrays were fabricated by depositing gold on CPI film with customized mask in the ion sputter (KYKY SBC-12). Then a microstructured dielectric layer of 14 × 14 $mm^2$ was packed between bottom electrode and top electrode arrays.

2.6. Characterization and Measurements:

The morphologies and microstructures of the samples were observed by field emission scanning electron microscope (FEI Quanta 650). Transmittance spectrum were taken by an ultraviolet-visible spectrophotometer (METASH, UV-5100). The sheet resistance was measured by four-point probe measurement (Model RTS-8, Four Probes Tech). The capacitance of sensor was measured by LCR meter (IM3523, HIOKI) with a testing frequency of 200 kHz. The external pressure was applied using a force gauge (AIGU-ZP-200, ETOOL Co., Ltd) with

a customized control stage (42BYGH4812AA, Huisitong Co., Ltd ). For cyclic loading/unloading tests, the sensor was placed on the testing system, and a constant pressure of 0.11 kPa was repeatedly applied and released while the electrical signals were recorded. For the bending test, the resistance of electrode was measured by Digit Multimeter (Agilent, 34401A).

2.7. Simulation:

A three-dimensional model and numerical simulations were performed using COMSOL (Multiphysics 5.2). The original height and diameter of micropillars were 11 μm and 5 μm, respectively. To simplify the simulation processes, the AgNWs film was ignored. The material properties such as density, Young's modulus, and Poisson's ratio were assigned as default value in the material library of COMSOL. A load was applied at the top of PDMS layer, and the applied load was gradually increased from (I) to (IX).

## 3. Results and Discussion

*3.1. Fabrication and characterization*

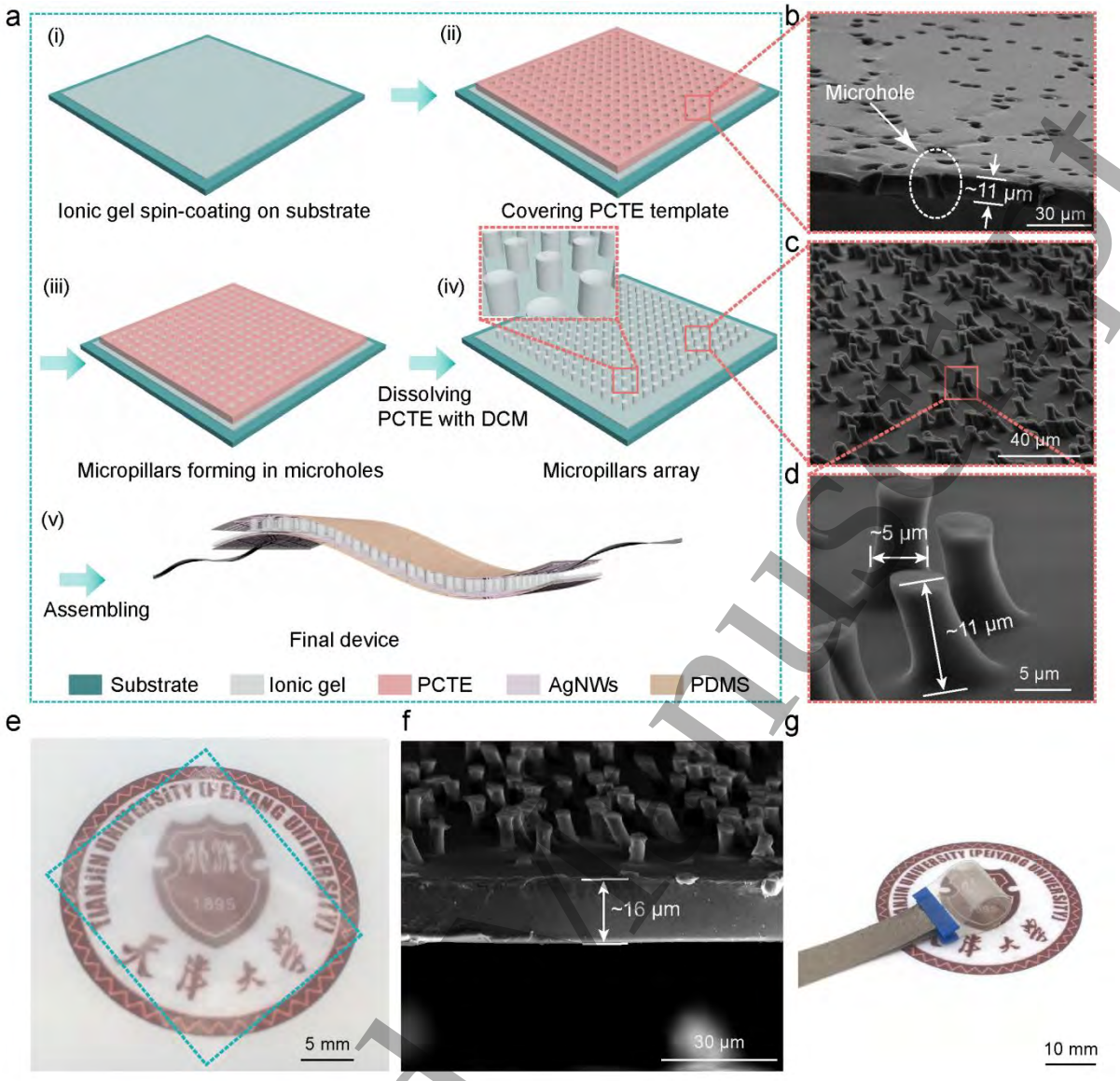


Figure 1. Schematic illustration of fabrication procedures and characterizations of flexible ionic pressure sensors. (a) Schematic illustration of fabrication procedures of ionic pressure sensor. (b) Tilt view SEM image of PCTE. (c) Tilt view SEM image and (d) its enlarged SEM image of micropillar array fabricated by template molding from PCTE. (e) Photo image of microstructured dielectric layer of ionic gel. (f) Sectional view of dielectric layer. (g) Photo image of ionic pressure sensor.

The fabrication procedures of flexible ionic pressure sensor are illustrated in Figure 1a. Firstly, an uncured ionic gel layer was spin-coated on the glass substrate and then a PCTE with lots of through microholes was placed on the surface of ionic gel layer immediately. Then the ionic gel was driven into the microholes of the PCTE from bottom to up by capillary force,

forming the micropillar array of ionic gel. At the top of micropillars, concave menisci were formed due to the lower surface tension of ionic gel. Following that ionic gel was dried in vacuum oven at 80 °C for 24h, the PCTE was dissolved with DCM and the ionic dielectric layer with microstructure was obtained. Detailed procedures can be seen in the Experiment Section. As shown in Figure S1, to prepare bottom and top electrodes, AgNWs solution was rod-coated on a hydrophilic PDMS film, which was achieved by treating with ultraviolet ozone. After rod-coating for several times, the electrode exhibits a low sheet resistance below 3 $\Omega \cdot sq^{-1}$ (Figure S2a). As shown in Figure S2b, the AgNWs electrode exhibits excellent robustness that leads to small resistance changes even after repeated bending for 3000 times. Finally, the top electrode, dielectric layer and bottom electrode were assembled into the entire device, forming the configuration of PDMS/AgNWs/dielectric layer/AgNWs/PDMS.

Figure 1b presents the tilt view scanning electron microscope (SEM) image of a PCTE, which exhibits scattered microholes with a thickness of ~11 μm. Figure S3a to S3c also shows images of PCTE captured by various methods. According to the results of random statistical distribution (Figure S3d), the diameters of the microholes follows a Laplace distribution with an average diameter of ~5 μm. The homogeneity within a template and template-to-template is also excellent according to Figure S4, Figure S5, Table S1 and Table S2, which are in the supplementary file alongside this article. Owing to the capillary action, the microholes of PCTE can be spontaneous filled with uncured ionic gel. After dissolving the PCTE , most micropillars kept upright and a few of micropillars cluster were formed because of capillary action between adjacent micropillars [30,31] (Figure 1c). The enlarged view indicates that the diameter of the bases of micropillars are larger than the top (Figure 1d), leading to promising mechanical robustness of the micropillars and capability to withstand repeated pressure. Furthermore, as presented in the Figure 1d, concave menisci are formed at the top of micropillars because adhesion force between ionic gel and PCTE is larger than cohesion force of ionic gel [32]. The

further characterization of concave meniscus and detailed mechanism is shown in Figure S6 and Section S1, respectively. The top-view SEM images of micropillars array and PCTE filled with ionic gel are shown in Figure S8 and Figure S9, respectively. It can be seen that microholes of PCTE was filled with ionic gel and concave menisci were formed at the top of micropillars. There are a few cracks in the microholes due to the reducing of the micropillar volume after solvent was evaporated. Thanks to the bottom-up manufacturing method, the ultrathin dielectric layer with an substrate of 16 μm can be obtained and it shows high transparency of 86% (Figure 1e, 1f and Figure S10). After packaging the top electrode, dielectric layer and bottom electrode, the entire device exhibits a transparency of 61% (Figure S10). Excellent performance in optical transparency may render this sensor the potential in being incorporated into the multicomponent systems of wearable devices [33].

*3.2. Mechanism and simulation*

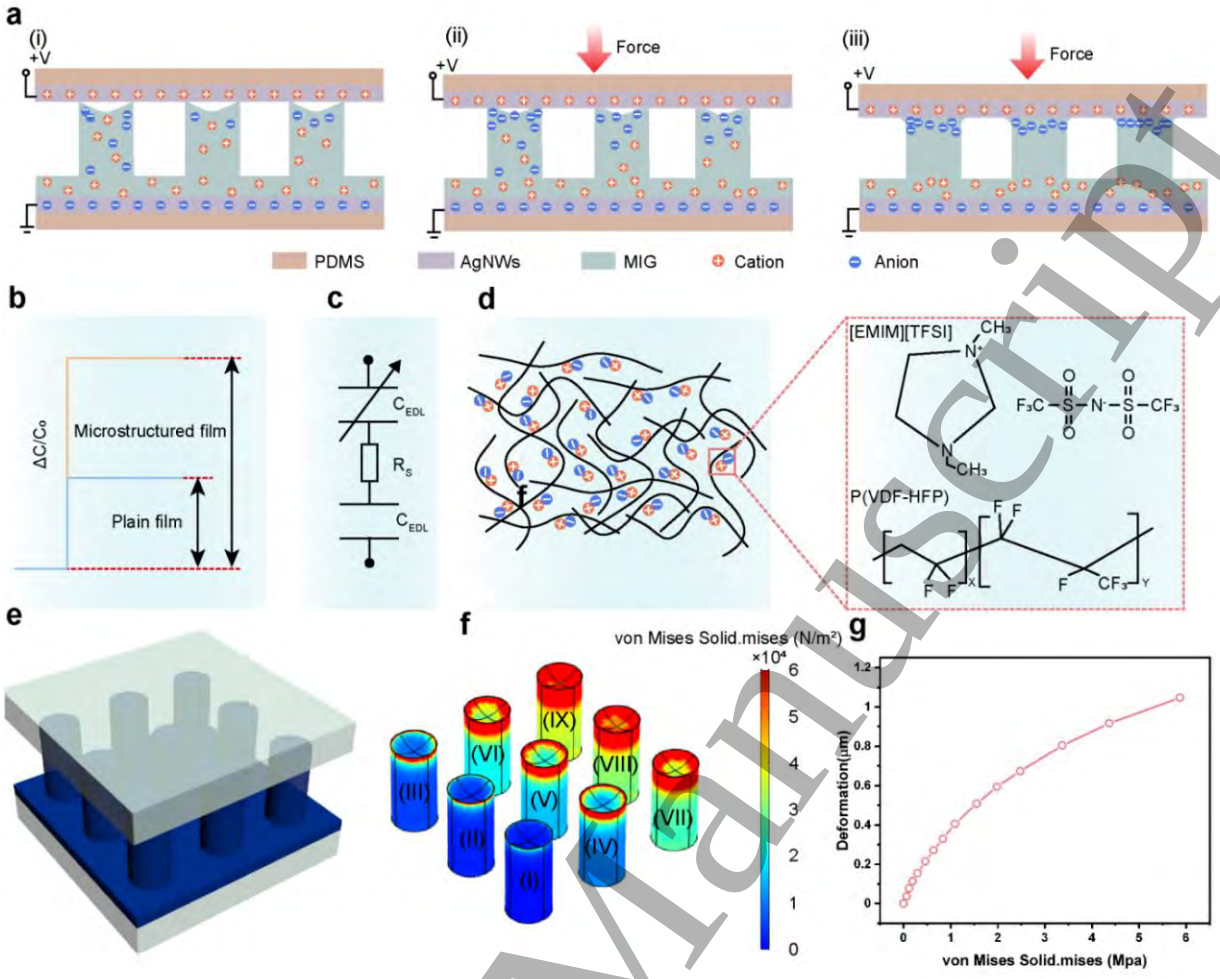


Figure 2. Illustration of sensing mechanism and simulation of stress distribution. (a) Schematic illustration of the sensing mechanism of the sensor. (b) An illustration of the relative change in the interfacial capacitance of the sensor under an external pressure for the microstructured ionic film and its unstructured counterpart. (c) Equivalent circuit model for the EDL (d) Chemical structures of the matrix and the IL:[EMIM][TFSI] and P(VDF-HFP). (e) The simulation model of micropillar array. (f) Simulation of stress distribution of micropillars with concave menisci at the top. (g) The von Mises Solid.mises increases with applied pressure.

The electrical properties of ionic gel and microstructure of concave meniscus play critical roles to the sensing performance of the ionic pressure sensor. As illustrated in Figure 2a, the microstructured dielectric layer of ionic gel is sandwiched between bottom and top AgNW/PDMS electrodes in a parallel configuration. The ionic film features with distributed massive low molar positive and negative charged ion pairs [34]. Therefore, an ionic-electronic

capacitive interface (or electrical double layers, EDL) was formed when a bias voltage is applied on electrodes and then the counter ions in the ionic film and the electrons in the electrodes accumulate and attract to each other at a nanometer distance [35]. The capacitance of EDL is determined by the contact area of the ionic-electronic capacitive interface. At an unloading state, the contact area is confined to the top edges of the concave menisci, leading to low initial capacitance. With the applied pressure increasing, contact area of ionic-electronic interface also expands. Compared with a plain ionic film, the relative change in capacitance of a microstructured ionic film is more substantial when equal pressure was applied, as illustrated in Figure 2b. The remarkedly larger capacitance change of microstructured ionic film is ascribed to that the deformation of microstructured film is more significant than a plain film. Thus the microstructure plays an important role in improving the performance of sensor. The entire sensor can be simplified as an EDL capacitors formed at the electrode/electrolyte interface connected with a bulk resistance in series according to the theory of Gouy-Chapman-Sterm model [36] (Figure 2c). The chemical structures of the ionic liquid based on 1-Ethyl-3-methylimidazolium (EMIM) cations, bis(trifluoromethane)sulfonimide (TFSI) anions, and the P(VdF-HFP) copolymer is shown in Figure 2d. The copolymer offers a framework for [EMIM] cations and [TFSI] anions as well as endows ionic film with excellent mechanical robustness.

As a demonstration of concept, Figure 2e-g presents the simulation results of microstructured ionic film against increasing pressure applied on the sensor. The contact area of the ionic-electronic interface is proportional to the deformation of the concave menisci. As illustrated in the Figure 2f, the pressure applied on micropillars increases gradually from I to IX thus the stress on micropillars also increases correspondingly. The stress initially concentrates on the edges of concave menisci, followed by gradual increase on the lateral faces with increased pressure. Figure 2g presents the deformation amplitude of concave menisci increases with the stress on them. In the lower regime of stress, the increment of deformation amplitude is

relatively fast because the Young's modulus of the top edge of concave menisci is low. However, with the improvement of deformation amplitude, the stress of concave menisci ascends slowly owing to the higher Young's modulus of low part of concave menisci. With the deformation amplitude of concave meniscus increasing, more area of concave meniscus contacts with electrode, leading higher capacitance of ionic-electronic interface.

The property of electrode such as the density of AgNWs network significantly influences the performance of the sensor. As shown in Figure S11a and S11b, the density of AgNWs network can be tuned by adjusting the cycles of rod-coating. With the resistance of electrode increasing from ~2.9 to ~300 $\Omega \cdot sq^{-1}$, the performance of transparency decreases from 98% to 62% (Figure S11c). Furthermore, the sensitivity of the sensor can be improved by dense AgNWs electrode as presents in Figure S11d. Different from conductive films that are consistent everywhere, the AgNWs electrode consists of lots of independent AgNWs, thus the contact area of ionic-electronic interface increases with the density of AgNWs network.

*3.3. Sensing performance*

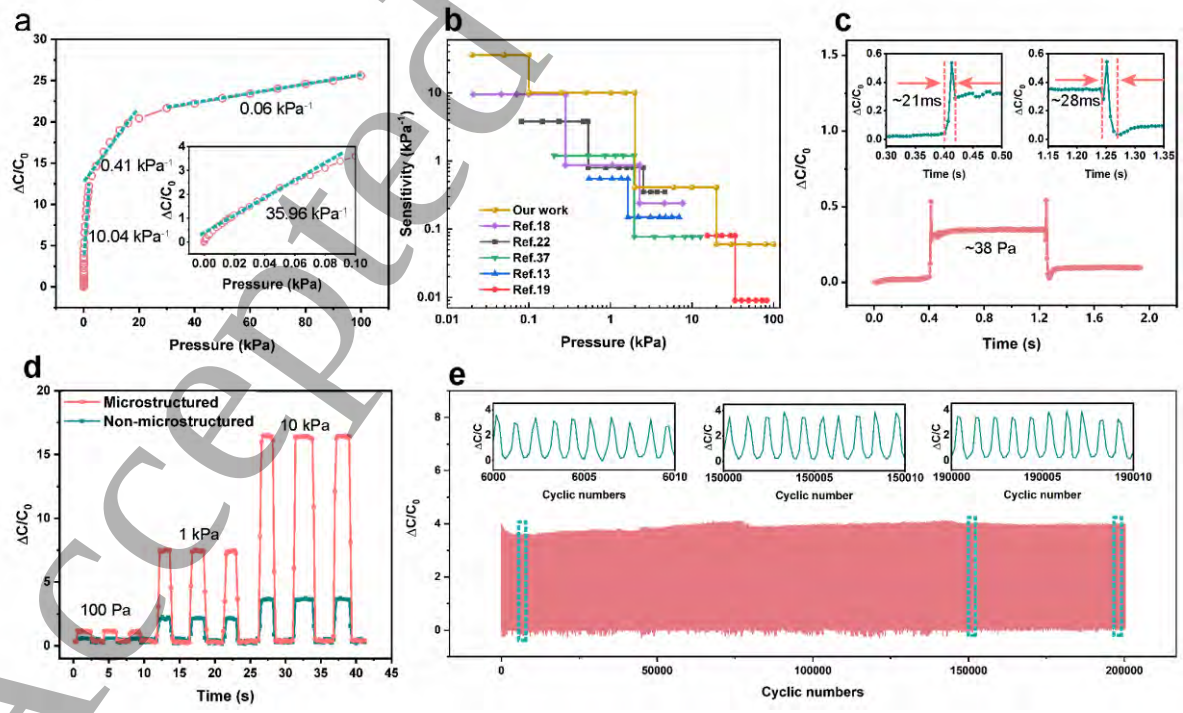

Figure 3. (a) The averaged change in capacitance as a function of pressure. Insert shows the change in capacitance as a function of pressure within 0.1 kPa. The standard deviation of capacitance change is extremely small to see. (b) Comparison of sensitivity of our sensor and the sensors in previous reported literatures. (c) Real-time response of the sensor to a pressure of ~38 Pa. Inserts present the response time upon loading and unloading. d) Repeated real-time responses of the sensor to the pressure of 0.1, 1, and 10 kPa. e) Mechanical robustness of the sensor tested for 200 000 cycles under an applied pressure of 0.11 kPa, and inserts show signals under different numbers of cycles.

The sensing performance of the ionic pressure sensor are evaluated in Figure 3. According to the pressure range of gentle finger touch (0 - 10 kPa) and daily body motion (10 - 100 kPa), the pressure range of testing is set to cover the pressure range of 0 - 100 kPa. The pressure of specific values were applied by a force gauge, and the corresponding capacitances of sensor were measured by a LCR meter. Then the change of capacitance was plotted against pressure and the sensitivity can be calculated by the equation $S = \delta(\Delta C/C_0)/\delta P$, where $C_0$ is the initial capacitance, $\Delta C$ is the change of capacitance ($C$-$C_0$), and P is the applied pressure. As for our sensor, the initial capacitance is ~22 pF at a frequency of 200 kHz. It is noted that the capacitance of ionic sensor decreases with the increasing frequency and reaches a relatively steady value at the frequency of 200 kHz. We are able to calculate the sensitivity of ionic pressure sensor by depicting the tangent of the curve of pressure response. As shown in Figure 3a, there are four different stages of sensitivity of our sensor. In the pressure regime of 0 - 0.1 kPa, the sensor achieves the sensitivity of 35.96 $kPa^{-1}$, endowing the sensor with the ability of perceiving tiny touch or pressure. With the pressure increasing, the sensitivity decreases gradually and the sensitivities are 10.04 $kPa^{-1}$ and 0.41 $kPa^{-1}$ in the 0.1 - 2 kPa and 2 - 20 kPa, respectively. In the pressure range of 20 - 100 kPa that is the pressure regime of daily body motion, the sensitivity still up to 0.06 $kPa^{-1}$, which satisfies the precision requirement for the detection of body motion as well as avoids unnecessary signal noise. Compared with previous reported results of microstructured pressure sensors as shown in Figure 3b [13,18,19,22,37],

our ionic microstructured pressure sensor exhibits comprehensive higher sensitivity in the pressure range of 0 - 100 kPa. Furthermore, the ionic pressure sensor presents the sensitivity of 0.06 $kPa^{-1}$ in the pressure regime of 20 - 100 kPa, which exceeds the effective responding range of many reported pressure sensors.

To investigate the response time of the ionic pressure sensor, a quarter of cover slide was loaded on its surface (10 × 10 $mm^2$), and the result is shown in Figure 3c. When the sensor was loaded with the object, the capacitance ascended rapidly to a stable value within a fast response time of ~21 ms, which is faster than the response time of human skin (30 - 50 ms). The time of returning to initial capacitance value is ~28 ms when the object was removed from the surface of the sensor. The difference of response time between loading and unloading might be ascribed to that the experimental operation of unloading is slower than loading [26]. When loaded with a scrap of paper of 0.61 Pa, the sensor can response to it clearly (Figure S12). Therefore, the limit of detection of the sensor is at least 0.61 Pa. Furthermore, to evaluate the repeatability of the sensor, the real-time responses of the sensor was tested with quick loading/unloading pressures of 0.2, 1 and 4 kPa for three circles each (Figure 2d). The results present that the microstructured sensor has stable responses with a high sensitivity as well as great repeatability. The pressure resolution of the sensor was characterized to demonstrate its ability to discriminate tiny pressure increment. As shown in Figure S13, in the pressure range of 3 - 23 Pa, the increment of 2 Pa can be clearly measured. Meanwhile, the increment of 3 Pa and 4 Pa also can be obviously distinguished in the pressure range of 200 - 230 Pa and 965 - 1050 Pa, respectively. The mechanical robustness of the sensor also was tested by repeatedly loading and unloading a pressure of 0.1 kPa for 200 000 times, and the results show the sensor maintains its function without obvious fatigue (Figure 2e). The signals in three different stages present quite similar waveforms as shown in the insets of Figure 2e and the results further indicate there is no obvious fatigue after 200 000 cycles. To our best knowledge, this is the largest cycle number of fatigue

test carried on a flexible capacitive sensor. Also the prssure responses at different locations of the sensor is almost the same (Figure S14), indicating the dielectric layer of the pressure sensor has an uniform microstructure so that the capacitance changes caused by the same pressure are identical. The thermal stability of ionic pressures sensor was characterized as shown in Figure S15. Within the range of room temperature (25 ℃) to 70 ℃, the capacitance of ionic sensor changes about 60% compared with initial capacitance (Figure S15). The increase of capacitance may is leaded by the heat-caused deformation of microstructure of dielectric layer. Also, the attraction force between cations and anions is decreased by the increased temperature [38]. Furthermore, compared with the reported results in former literatures (Table S3), our sensor shows comprehensive performance in high sensitivity, low LOD, good stability and reliability, although not the best in all aspects.

*3.4. Practical applications*

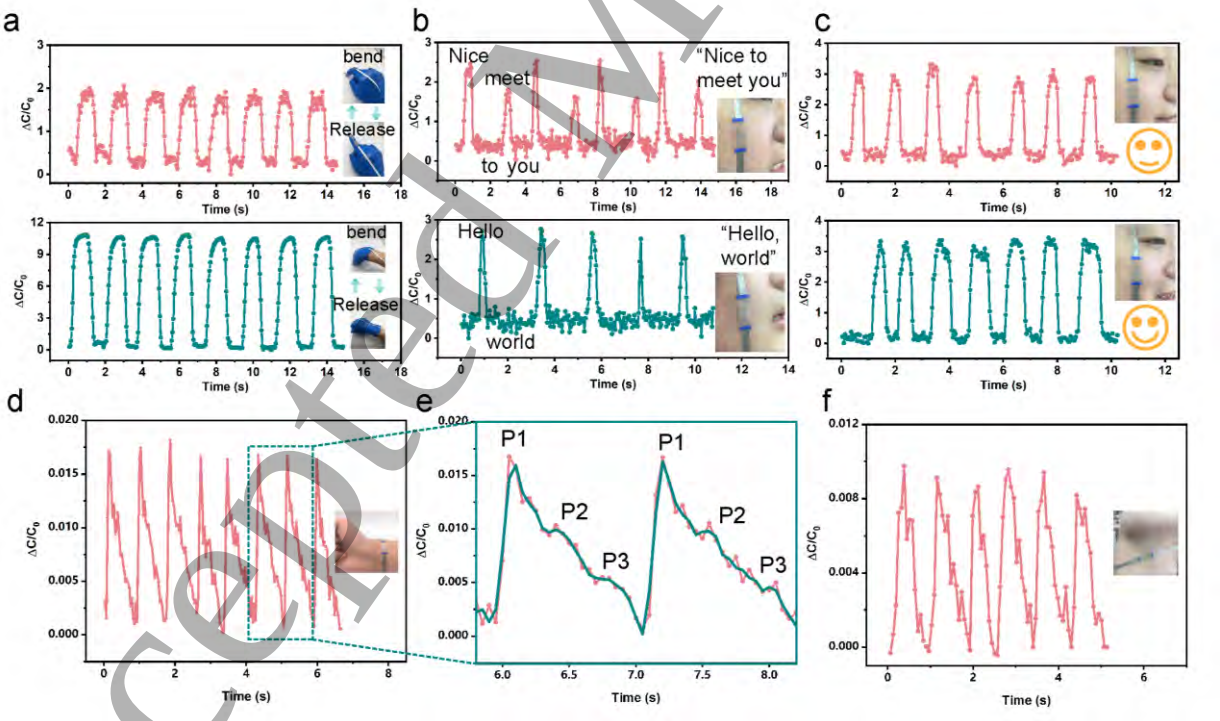


Figure 4. (a) Capacitance change of the sensor with finger touch and wrist bending. (b) Capacitance change of the sensor in the demonstration of speaking detection. (c) Demonstration of smile detection, including smile and laugh. (d) Detection of wrist pulse and (e) its enlarged

figure of two waves. (f) Detection of pulse at superficial temporal artery.

To demonstrate the capability of dynamic interaction with human or environmental stimulus, repeated finger touches and wrist bendings were applied on the ionic pressure sensor. As shown in Figure 4a, the cyclical pattern of capacitance change clearly indicates periodic finger touches and wrist bendings. In addition, when the sensor was attached to the face of tester, it is able to monitor the muscle motion of the face caused by speaking (Figure 4b). Furthermore, the sensor can distinguish between smile and laugh through the waveform pattern of capacitance change, as shown in Figure 4c. Pulses such as wrist pulse and neck pulse is one of relatively tiny vibrations of human being, however, our sensor can detect these kinds of biological signals accurately, as presented in Figure 3d-f. In addition to precise detection of global pattern of pulse, the ionic sensor can distinguish extremely small change of flow rate of blood, which is named main peak (P1), predicrotic peak (P2) and dicrotic peak (P3), respectively. The demonstration of pulse meter at superficial temporal artery further exhibits its versatility in biological applications, avoiding the restriction of location in usage of sensors.

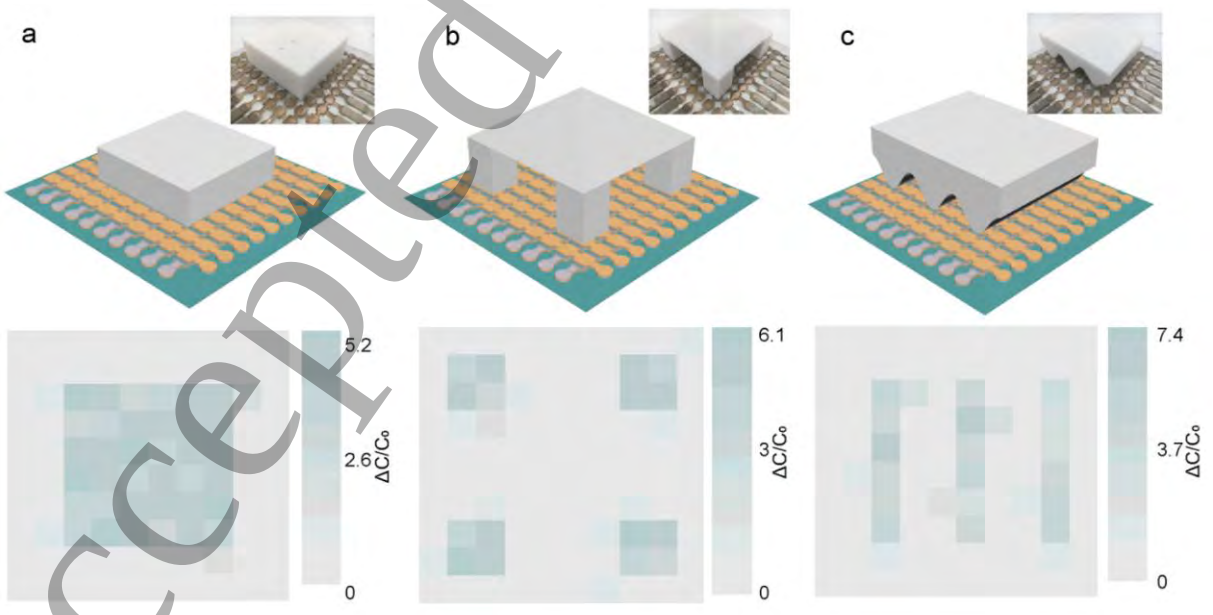

Figure 5. Demonstration of pressure mapping for the ionic sensor array using (a) cuboid, (b) quadrilateral pyramid with four legs and (c) wave-like shape.

In order to mimic the capability of two-dimensional pressure sensing of human skins, the ionic pressure sensor array was developed to enable the pressure mapping. Taking advantages of the convenience and operability of the manufacturing method, we readily scaled up the sensor layouts to an array configuration with required pixels of 10 × 10 to collect the spatial pressure information. The manufacturing procedures of the ionic pressure sensor array is schematically illustrated in Figure S16 (Detail procedures in Experimental Section). When a cuboid of poly lactic acid was placed on the sensor array, the capacitance change of pixels array is capable to literally represents the object silhouette and the color contrast maps local pressure distribution (Figure 5a). In addition, the sensor array also can distinguish different patterns of quadrilateral pyramid with four legs and wave-like shape according to silhouette reflected by capacitance change (Figure 5b-c). These results present that the ionic pressure sensor array has the potential to map external pressures like our skin and can be utilized in the wearable electronics.

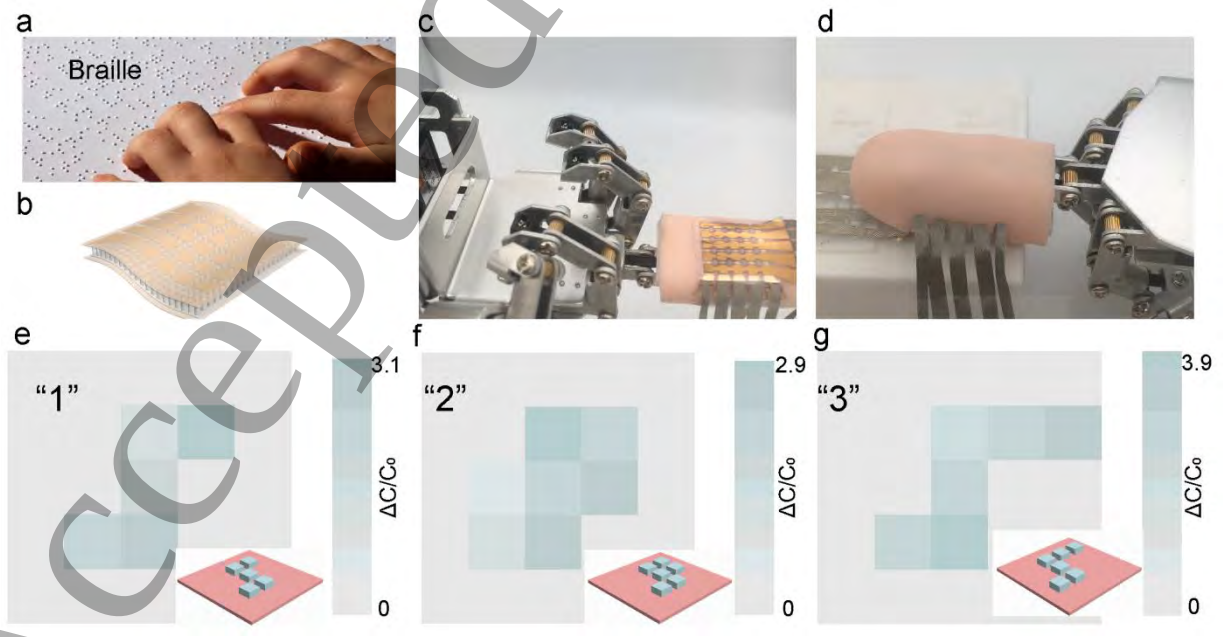

Figure 6. Demonstration of pressure mapping for the ionic sensor array of high spatial resolution using braille numbers. (a)The photo image of recognition of braille alphabets. (b) Illustration of ionic sensor array of high spatial resolution. (c) Photo image of sensor array attached to the finger of robot. (d) Photo image of configuration for the recognition of braille numbers. Pressure mapping of braille numbers of (e) "1", (f) "2" and (g) "3".

High spatial resolution of pressure sensor is essential for a few applications such as the recognition of braille alphabets (Figure 6a). Although the pressure mapping is realized with pressure sensor array, the limited resolution still is an obstacle in such applications. Thanks to the high sensitivity of the ionic sensor and the convenience of the manufacturing method, an ionic pressure sensor array with a high spatial resolution of $2.8 \times 2.8$ mm$^2$ was achieved (Figure S17). It has 25 independent detection units located in the area of $14 \times 14$ mm$^2$ (Figure 6b). In order to recognize braille alphabets accurately, the ionic pressure sensor array was attached to the finger of robot and then touch the braille number on the substrate as shown in Figure 6c-d. The pressure mapping and color contrast is shown in Figure 6e-g, which exhibits the capability of high spatial resolution for recognition of braille alphabets. These results indicates our ionic pressure sensor array has a promising potential in pressure mapping with a high spatial resolution, not limited in recognition of braille numbers.

## 4. Conclusion

In conclusion, we have developed a highly sensitive ionic capacitive pressure sensor with bottom-up template method. Concave menisci were formed at the top of micropillar array therefore remarkable capacitance change can be realized when a pressure is applied. The sensor presents a high sensitivity of 35.96 k Pa$^{-1}$ and can be repeatedly tested for at least 200 000 cycles. In addition, the response time is 21 ms and the limit of detection is 0.61 Pa. These results indicate the promising potential of the sensor for various applications in human-machine interaction. The manufacturing method for capillary-driven concave meniscus may provide a novel method for sensing device in wearable electronics.

**Acknowledgements**

This work was supported by the Project Technologically Beneficial to People of Qiangdao (China) (17-3-3-90-nsh). The authors would like to thank Shiyanjia Lab (www.shiyanjia.com/) for the support of SEM test.

**References**

[1] Hua Q, Sun J, Liu H, Bao R, Yu R, Zhai J, Pan C and Wang Z L 2018 Skin-inspired highly stretchable and conformable matrix networks for multifunctional sensing Nat. Commun. 9

[2] Boutry C M, Negre M, Jorda M, Vardoulis O, Chortos A and Khatib O 2018 A hierarchically patterned, bioinspired e-skin able to detect the direction of applied pressure for robotics Sci. Robot. 10

[3] Hammock M L, Chortos A, Tee B C-K, Tok J B-H and Bao Z 2013 The Evolution of Electronic Skin (E-Skin): A Brief History, Design Considerations, and Recent Progress Adv. Mater. 25 5997-6038

[4] Zhan Z, Lin R, Tran V-T, An J, Wei Y, Du H, Tran T and Lu W 2017 Paper/Carbon Nanotube-Based Wearable Pressure Sensor for Physiological Signal Acquisition and Soft Robotic Skin ACS Appl. Mater. Interfaces 9 37921–8

[5] Larson C, Peele B, Li S, Robinson S, Totaro M, Beccai L, Mazzolai B and Shepherd R 2016 Highly stretchable electroluminescent skin for optical signaling and tactile sensing Science 351 1071-4

[6] Huang Y, Fan X, Chen S and Zhao N 2019 Emerging Technologies of Flexible Pressure Sensors: Materials, Modeling, Devices, and Manufacturing Adv. Funct. Mater. 29 1808509

[7] Guo Y, Guo Z, Zhong M, Wan P, Zhang W and Zhang L 2018 A Flexible Wearable Pressure Sensor with Bioinspired Microcrack and Interlocking for Full-Range Human-Machine Interfacing Small 14 1803018

[8] Liu S, Wu X, Zhang D, Guo C, Wang P, Hu W, Li X, Zhou X, Xu H, Luo C, Zhang J and Chu J 2017 Ultrafast Dynamic Pressure Sensors Based on Graphene Hybrid Structure ACS Appl. Mater. Interfaces 9

24148-54

[9] Huang Y, Chen Y, Fan X, Luo N, Zhou S, Chen S-C, Zhao N and Wong C P 2018 Wood Derived Composites for High Sensitivity and Wide Linear-Range Pressure Sensing Small 14 1801520

[10] Wang X, Liu Z and Zhang T 2017 Flexible Sensing Electronics for Wearable/Attachable Health Monitoring Small 13 1602790

[11] He Z, Chen W, Liang B, Liu C, Yang L, Lu D, Mo Z, Zhu H, Tang Z and Gui X 2018 Capacitive Pressure Sensor with High Sensitivity and Fast Response to Dynamic Interaction Based on Graphene and Porous Nylon Networks ACS Appl. Mater. Interfaces 10 12816-23

[12] Luo Y, Shao J, Chen S, Chen X, Tian H, Li X, Wang L, Wang D and Lu B 2019 Flexible Capacitive Pressure Sensor Enhanced by Tilted Micropillar Arrays ACS Appl. Mater. Interfaces 11 17796-803

[13] Mannsfeld S C B, Tee B C-K, Stoltenberg R M, Chen C V H-H, Barman S, Muir B V O, Sokolov A N, Reese C and Bao Z 2010 Highly sensitive flexible pressure sensors with microstructured rubber dielectric layers Nat. Mater. 9 859-64

[14] Cho S H, Lee S W, Yu S, Kim H, Chang S, Kang D, Hwang I, Kang H S, Jeong B, Kim E H, Cho S M, Kim K L, Lee H, Shim W and Park C 2017 Micropatterned Pyramidal Ionic Gels for Sensing Broad-Range Pressures with High Sensitivity ACS Appl. Mater. Interfaces 9 10128-35

[15] Chhetry A, Kim J, Yoon H and Park J Y 2019 Ultrasensitive Interfacial Capacitive Pressure Sensor Based on a Randomly Distributed Microstructured Iontronic Film for Wearable Applications ACS Appl. Mater. Interfaces 11 3438-49

[16] Zhang H Z, Tang Q Y and Chan Y C 2012 Development of a versatile capacitive tactile sensor based on transparent flexible materials integrating an excellent sensitivity and a high resolution AIP Adv. 2 022112

[17] Lee K, Lee J, Kim G, Kim Y, Kang S, Cho S, Kim S, Kim J-K, Lee W, Kim D-E, Kang S, Kim D, Lee T and Shim W 2017 Rough-Surface-Enabled Capacitive Pressure Sensors with 3D Touch Capability Small 13 1700368

[18] Yoon S G, Park B J and Chang S T 2017 Highly Sensitive Piezocapacitive Sensor for Detecting Static

and Dynamic Pressure Using Ion-Gel Thin Films and Conductive Elastomeric Composites ACS Appl. Mater. Interfaces 9 36206-19

[19] Kang S, Lee J, Lee S, Kim S, Kim J-K, Algadi H, Al-Sayari S, Kim D-E, Kim D and Lee T 2016 Highly Sensitive Pressure Sensor Based on Bioinspired Porous Structure for Real-Time Tactile Sensing Adv. Electron. Mater. 2 1600356

[20] Yang X, Wang Y, Sun H and Qing X 2019 A flexible ionic liquid-polyurethane sponge capacitive pressure sensor Sens. Actuator A-Phys. 285 67-72

[21] Sun K, Ko H, Park H-H, Seong M, Lee S-H, Yi H, Park H W, Kim T, Pang C and Jeong H E 2018 Hybrid Architectures of Heterogeneous Carbon Nanotube Composite Microstructures Enable Multiaxial Strain Perception with High Sensitivity and Ultrabroad Sensing Range Small 14 1803411

[22] Joo Y, Byun J, Seong N, Ha J, Kim H, Kim S, Kim T, Im H, Kim D and Hong Y 2015 Silver nanowire-embedded PDMS with a multiscale structure for a highly sensitive and robust flexible pressure sensor Nanoscale 7 6208-15

[23] Hu W, Niu X, Zhao R and Pei Q 2013 Elastomeric transparent capacitive sensors based on an interpenetrating composite of silver nanowires and polyurethane Appl. Phys. Lett. 102 083303

[24] Yin X-Y, Zhang Y, Cai X, Guo Q, Yang J and Lin Wang Z 2019 3D printing of ionic conductors for high-sensitivity wearable sensors Mater. Horizons 6 767-80

[25] Wang H, Wang Z, Yang J, Xu C, Zhang Q and Peng Z 2018 Ionic Gels and Their Applications in Stretchable Electronics Macromol. Rapid Commun. 39 1800246

[26] Qiu Z, Wan Y, Zhou W, Yang J, Yang J, Huang J, Zhang J, Liu Q, Huang S, Bai N, Wu Z, Hong W, Wang H and Guo C F 2018 Ionic Skin with Biomimetic Dielectric Layer Templated from Calathea Zebrine Leaf Adv. Funct. Mater. 28 1802343

[27] Choi D, Jang S, Kim J S, Kim H-J, Kim D H and Kwon J-Y 2019 A Highly Sensitive Tactile Sensor Using a Pyramid-Plug Structure for Detecting Pressure, Shear Force, and Torsion Adv. Mater. Technol. 4 1800284

[28] Jang S, Jee E, Choi D, Kim W, Kim J S, Amoli V, Sung T, Choi D, Kim D H and Kwon J-Y 2018 Ultrasensitive, Low-Power Oxide Transistor-Based Mechanotransducer with Microstructured, Deformable Ionic Dielectrics ACS Appl. Mater. Interfaces 10 31472-9

[29] Chandra D and Yang S 2009 Capillary-Force-Induced Clustering of Micropillar Arrays: Is It Caused by Isolated Capillary Bridges or by the Lateral Capillary Meniscus Interaction Force Langmuir 25 10430-4

[30] Chandra D and Yang S 2009 Capillary-Force-Induced Clustering of Micropillar Arrays: Is It Caused by Isolated Capillary Bridges or by the Lateral Capillary Meniscus Interaction Force? Langmuir 25 10430–4

[31] Chandra D and Yang S 2010 Stability of High-Aspect-Ratio Micropillar Arrays against Adhesive and Capillary Forces Acc. Chem. Res. 43 1080-91

[32] a) Rao K J, Li F, Meng L, Zheng H, Cai F and Wang W 2015 A Force to Be Reckoned With: A Review of Synthetic Microswimmers Powered by Ultrasound Small 11 2836-46; b) Megias-Alguacil D and Gauckler L J 2009 Capillary forces between two solid spheres linked by a concave liquid bridge: Regions of existence and forces mapping AIChE J. 55 1103-9; c) Hillel D 1998 Environmental Soil Physics (San Diego: Elsevier)

[33] Kim S-R, Kim J-H and Park J-W 2017 Wearable and Transparent Capacitive Strain Sensor with High Sensitivity Based on Patterned Ag Nanowire Networks ACS Applied Materials & Interfaces 9 26407-16

[34] Nie B, Li R, Cao J, Brandt J D and Pan T 2015 Flexible Transparent Iontronic Film for Interfacial Capacitive Pressure Sensing Advanced Materials 27 6055-62

[35] a) Nie B, Xing S, Brandt J D and Pan T 2012 Droplet-based interfacial capacitive sensing Lab Chip 12 1110–8; b) Keplinger C, Sun J-Y, Foo C C, Rothemund P, Whitesides G M and Suo Z 2013 Stretchable, Transparent, Ionic Conductors Science 341 984-7

[36] Oldham K B, 2008 A Gouy-Chapman-Stern model of the double layer at a (metal)/(ionic liquid) interface J. Electroanal. Chem. 613 131-8

[37] Wan Y, Qiu Z, Hong Y, Wang Y, Zhang J, Liu Q, Wu Z and Guo C F 2018 A Highly Sensitive Flexible Capacitive Tactile Sensor with Sparse and High-Aspect-Ratio Microstructures Adv. Electron. Mater. 4 1700586

[38] Higa M and Yamakawa T 2004 Design and Preparation of a Novel Temperature-Responsive Ionic Gel.

1. A Fast and Reversible Temperature Response in the Charge Density J. Phys. Chem. B 108 16703–7